Springer Proceedings in Physics 400

Chao Chang
Yaxin Zhang
Ziran Zhao
Yiming Zhu *Editors*

Proceedings of the 5th China and International Young Scientist Terahertz Conference, Volume 1

YTHZ 2024, 22–24 March, Chengdu, China

Springer

Springer Proceedings in Physics **400**

Indexed by Scopus

The series Springer Proceedings in Physics, founded in 1984, is devoted to timely reports of state-of-the-art developments in physics and related sciences. Typically based on material presented at conferences, workshops and similar scientific meetings, volumes published in this series will constitute a comprehensive up to date source of reference on a field or subfield of relevance in contemporary physics. Proposals must include the following:

- Name, place and date of the scientific meeting
- A link to the committees (local organization, international advisors etc.)
- Scientific description of the meeting
- List of invited/plenary speakers
- An estimate of the planned proceedings book parameters (number of pages/articles, requested number of bulk copies, submission deadline).

Please contact:

For Americas and Europe: Dr. Zachary Evenson; zachary.evenson@springer.com
For Asia, Australia and New Zealand: Dr. Loyola DSilva; loyola.dsilva@springer.com

Chao Chang · Yaxin Zhang · Ziran Zhao ·
Yiming Zhu
Editors

Proceedings of the 5th China and International Young Scientist Terahertz Conference, Volume 1

YTHZ 2024, 22–24 March, Chengdu, China

Springer

Editors
Chao Chang
Peking University
Beijing, China

Ziran Zhao
Tsinghua University
Beijing, China

Yaxin Zhang
University of Electronic Science
and Technology of China
Chengdu, China

Yiming Zhu
University of Shanghai for Science
and Technology
Shanghai, China

ISSN 0930-8989 ISSN 1867-4941 (electronic)
Springer Proceedings in Physics
ISBN 978-981-97-3785-7 ISBN 978-981-97-3786-4 (eBook)
https://doi.org/10.1007/978-981-97-3786-4

This Springer imprint is published by the registered company Springer Nature Singapore Pte Ltd.
The registered company address is: 152 Beach Road, #21-01/04 Gateway East, Singapore 189721, Singapore

Contents

THz Sensors and Detection

THz Sensors and Detection

Explosives Detection by Terahertz Spectroscopy and Artificial Neural Network

Sijia Li[1,2], Meng Chen[2], Yingxin Wang[1,2(✉)], and Ziran Zhao[1,2]

[1] Department of Engineering Physics, Tsinghua University, Beijing 100084, China
wangyingxin@tsinghua.edu.cn
[2] National Engineering Research Center for Dangerous Articles and Explosives Detection Technologies, Beijing 100084, China

Abstract. Terahertz spectroscopy can reveal the spectral fingerprint characteristics of different materials in the terahertz range, which allows distinguishing explosives from common materials. In this work, by using the terahertz spectrum as a feature vector to establish an artificial neural network recognition model, we successfully achieve the identification of explosives and conventional materials, as well as the determination of different explosive classes.

Keywords: Terahertz Spectroscopy · Explosives · Artificial Neural Network

1 Introduction

Thanks to the fingerprint characteristics of terahertz spectroscopy, qualitative identification and even quantitative detection of prohibited items have become possible [1–5]. The first key issue involved is what identification method to use to determine "whether" and "what" prohibited items are. The simplest way is to directly compare the spectrum of the tested material with the standard spectrum in the database. However, for practical applications, especially in the detection of hidden prohibited or packaged products, interference from obstructions and noise can complicate the spectrum and increase uncertainty. A more effective approach is to establish an identification model that contains as much spectral variation information as possible. The specific process is to design a classifier by training (or learning) a certain number of samples, and then make classification decisions for the identified samples. There are multiple pattern recognition techniques that can be selected as classification tools, among which artificial neural networks (ANNs) have strong nonlinear mapping ability and have been used for the recognition of terahertz spectra [2]. Here we present to use ANNs for explosives detection based on terahertz spectroscopy.

2 Sample Preparation

Four typical explosives, TNT, RDX, HMX, and Composition B (CB), as well as ten conventional materials, were selected for qualitative identification of prohibited items. The parameters and properties of each material are shown in Tables 1 and 2. In the experiment, the explosive samples were compressed into uniformly thick pellets to reduce

C. Chang et al. (Eds.): YTHZ 2024, SPPHY 400, pp. 3–7, 2024.
https://doi.org/10.1007/978-981-97-3786-4_1

the influence of scattering effects. All other materials were in their normal state and had not been pre-treated. A terahertz time-domain spectroscopy (THz-TDS) system was employed to test the terahertz spectra of various materials [6, 7]. To reduce the impact of water vapor absorption in the air, the THz-TDS system was filled with dry nitrogen, and the final relative humidity inside the system was around 4%.

Table 1. Explosive Samples and Their Properties

Explosives	Molecular formula	Thickness (mm)	Properties
TNT	$C_7H_5N_3O_6$	1.6	Light yellow scaly crystalline flakes, the most widely used military explosive
RDX	$C_3H_6N_6O_6$	1.0	White crystalline powder, commonly mixed with other explosive materials and plasticizers to make plastic explosives
HMX	$C_4H_8N_8O_8$	0.8	Homolog of RDX, white crystalline powder, commonly used as solid fuel for rocket propulsion and military warheads
CB	$C_7H_5N_3O_6/C_3H_6N_6O_6$	2.9	Mixed explosive formed by adding solid particles of RDX into molten TNT, widely used in military applications

Table 2. Non-Explosive Samples and Their Properties

Materials	Cloth	Towel	Leather	Plastic	Envelope
Thickness (mm)	0.6	~1.5	1.0	1.1	0.3
Color	Blue	Yellow	Black	Black	Yellow

Materials	Polyethylene	Foam	Paperboard	Flour	Soda ash
Thickness (mm)	2.1	3.2	0.5	~1.5	~1.5
Color	White	White	Gray	White	White

3 Experimental Results

ANN is a complex network formed by a large number of processing units (neurons) connected to each other. Its model is based on instance learning and adopts parallel reasoning methods, with features such as association, memory, and induction. The feed-forward neural network is one of the most widely and successfully applied networks in

the field of pattern recognition, represented by multi-layer perceptrons (BP networks) that use error backpropagation learning algorithms (BP algorithms). The BP network completes the nonlinear mapping from input signals to output modes through the mutual correlation between layers. The weight of the network is adjusted by the feedback of the error signal between the actual output and the expected output. The continuous correction of the weight gradually makes the actual output of the network closer to the expected output, thus completing the training process.

The feasibility of qualitatively identifying prohibited items through terahertz spectroscopy analysis is verified using BP network below. There are two tasks that need to be addressed here: one is to distinguish prohibited items from conventional materials, and the other is to identify the classes of prohibited items.

3.1 Distinguishing Between Explosives and Non-explosives

The training set was constructed by the spectra of RDX, HMX, TNT obtained from 5 measurements, as well as the spectra of ten non-explosive samples, containing a total of 25 samples. The test set includes 2 spectra of RDX, HMX, TNT, and CB measured at another time, 1 spectrum of RDX concealed in envelopes and fabrics (C-RDX), and 20 spectra of non-explosive samples collected at that time. To eliminate the influence of thickness, all spectra were normalized.

The BP network structure consists of three layers. The input layer has 124 nodes, corresponding to the spectral length within the effective frequency range. The hidden layer has 15 nodes, and the output layer has 1 node, corresponding to whether it is an explosive. The excitation function of the hidden layer in the network is the Sigmoid function $f(x) = 1/(1 + e^{-x})$, and the output layer is a linear function $f(x) = x$. . The training and testing of the network were implemented by the Neural Network Toolbox of Matlab (Mathworks Inc.). During training, set the output value of the network to 1 for explosive samples and 0 for non-explosive samples. The training algorithm adopted the Fletcher Reeves conjugate gradient algorithm, and the mean square error between the actual output and the expected output of the final network reached the predetermined accuracy (10^{-7}).

After training, the test set samples were used as input data to test the recognition performance of the network, as shown in Fig. 1. It can be seen that the output values of explosive and non-explosive samples are distributed around the target values of 1 and 0, respectively, which preliminarily verifies the recognition ability of the network. In order to calculate the recognition rate, a quantitative standard is needed. The deviation between the network output value y and the target output y_0 is defined as $\delta = |y - y_0|$, and a recognition threshold δ_0 is selected, that is, the recognition is considered correct when $\delta < \delta_0$, otherwise it is considered incorrect or the decision is rejected. At this point, the recognition rate can be defined as

$$\eta = \frac{\sum_{i=1}^{N} u(\delta_0 - \delta_i)}{N} \times 100\% \tag{1}$$

where N is the number of test samples and u is the threshold function. When $x < 0$, $u(x) = 0$. In cases of $\delta_0 = 5\%$ and $\delta_0 = 10\%$, the recognition rates are 80% and 95%,

respectively. The test results indicate that the use of terahertz spectroscopy and neural network methods can effectively distinguish explosives from conventional items to a certain extent.

Note that the training set does not include the spectra of C-RDX and CB, but the network still correctly recognizes them. Due to the lack of absorption characteristics in the spectra of conventional materials, the spectral characteristics of RDX can still be displayed in hidden situations, while CB is composed of a mixture of RDX and TNT, and its absorption spectrum reflects the characteristics of RDX. Therefore, the network successfully identifies it. This fully demonstrates that terahertz spectroscopy technology can effectively detect specific components in hidden prohibited substances and mixtures.

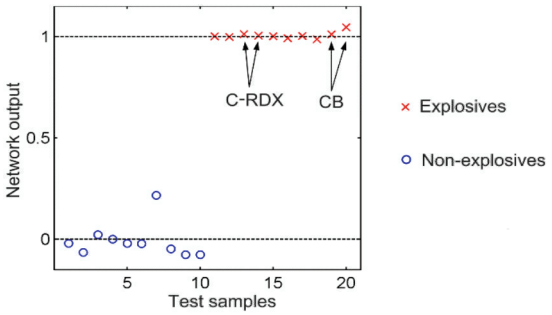

Fig. 1. BP network outputs for distinguishing between explosives and non-explosives.

3.2 Identification of Explosive Classes

On the basis of distinguishing between explosives and non-explosives, it is necessary to further distinguish the explosive classes. To achieve this purpose, a classification network was re-established using the spectra of explosive samples. The training set includes spectra of RDX, HMX, and TNT samples measured 10 times, and contains a total of 30 samples. The test set includes 5 spectra of RDX, HMX, TNT, and CB measured at another time, and 1 spectrum of RDX hidden in envelopes and fabrics, containing a total of 22 samples. The network structure was still divided into three layers, and the number of hidden nodes, excitation function, and training algorithm were the same as the previously constructed network. The difference is that the output layer has three neurons, corresponding to RDX, HMX, and TNT. When the output value is 1, it indicates the presence of the sample, while 0 indicates the absence. For example, [1 0 0], [0 1 0], and [0 0 1] represent RDX, HMX, and TNT, respectively.

The network response to the test set is shown in Fig. 2, which shows good discrimination among various explosives, and the output vectors of the same sample are tightly clustered together. According to the class decision method of multi output networks, samples of unknown classes were determined as the class corresponding to the node with the highest output value. Finally, all test samples of RDX, HMX, TNT, and C-RDX were correctly identified. In addition, due to the significant similarity in the spectra of

CB and RDX, while the TNT spectral features are not obvious, the network recognizes CB as RDX, which is understandable.

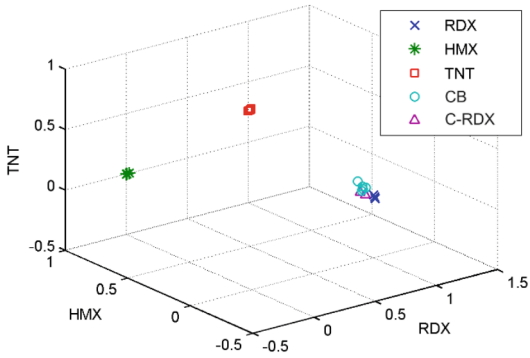

Fig. 2. BP network outputs for identification of explosive classes.

Through the above experiments, it can be seen that ANN can fully utilize all the information of terahertz spectrum for learning and quickly identify unknown samples. Its nonlinear prediction ability reduces the influence of system noise, which is conducive to improving the detection efficiency and recognition rate of the system.

Acknowledgment. This work was supported by the National Key R&D Program of China (No. 2023YFF0715000).

References

1. Kemp, M.: Explosives detection by terahertz spectroscopy—a bridge too far? IEEE Trans. Terahertz Sci. Technol. **1**(1), 282–292 (2011). https://doi.org/10.1109/TTHZ.2011.2159647
2. Wang, C., et al.: Convolutional neural network-based terahertz spectral classification of liquid contraband for security inspection. IEEE Sens. J. **21**(17), 18955–18963 (2021)
3. Liu, G., et al.: Myelin sheath as a dielectric waveguide for signal propagation in the mid-infrared to terahertz spectral range. Adv. Funct. Mater. **29**(7), 1807862 (2019)
4. Li, Y., et al.: Terahertz wave enhances permeability of the voltage-gated calcium channel. J. Am. Chem. Soc. **143**(11), 4311–4318 (2021)
5. Xiang, Z., et al.: A primary model of THz and far-infrared signal generation and conduction in neuron systems based on the hypothesis of the ordered phase of water molecules on the neuron surface. Sci. Bull. **65**, 308 (2020)
6. Wang, Y., et al.: Terahertz absorbance spectrum fitting method for quantitative detection of concealed contraband. J. Appl. Phys. **102**, 113108 (2007)
7. Wang, Y., et al.: THz technology using in exploring the recognition of explosives concealed on personnel. In: Proceedings of the 13th national academic annual conference nuclear electric detective Technology, vol. 397. China (2006)

High-Performance Infrared to Terahertz Detector Based on Topological Semimetal $ZrTe_3$

Guanchu Ding[1], Aosheng Zheng[1], Fan Yang[1], Zhengyi Zhao[1], Tan Qi[1], Yanyan Liu[2(✉)], Yating Zhang[1(✉)], and Jianquan Yao[1]

[1] Key Laboratory of Opto-Electronics Information Technology (Tianjin University), Ministry of Education, School of Precision Instruments and Opto-Electronics Engineering, Tianjin University, Tianjin 300072, China
yating@tju.edu.cn

[2] National Key Laboratory of Electromagnetic Space Security, Tianjin 300308, China
lyy13@126.com

Abstract. Terahertz radiation with applications in the field of medical diagnostics, astronomical remote sensing, imaging, biomedical research, communication etc. has been widely investigated recently. As a vital part of these applications, the development of terahertz photodetectors (PDs) is urgently needed. However, the widely investigated graphene and other two-dimensional materials for terahertz PD still facing optimal combination between bandgap, dark current, and absorption capabilities. Here, adopting the zero-bandgap and high carrier density characteristics of topological semimetals (TSMs), we applied the TSM $ZrTe_3$ for constructing high-performance terahertz PD. The PD achieved high responsivity of 0.11 A/W at 0.22 THz with response time of 4.74/4.97 ms, which exhibits great potentials for terahertz applications. Moreover, taking the zero-bandgap advantage of $ZrTe_3$, the PD was able to respond across ultra broad spectrum range spanning from near infrared to terahertz. The responsivity of the PD was recorded from near infrared to terahertz, confirming the broad band photodetection capability.

Keywords: Terahertz Detection · Photodetector · Topological Semimetals

1 Introduction

Terahertz radiation, refer to the electromagnetic wave within the wavelength of 0.03–3 mm (corresponding frequencies situated at 0.1–10 THz), possess significant application potentials in medical diagnostics, astronomical remote sensing, imaging, biomedical research, communication etc. [1–8]. Terahertz photodetectors (PDs) denote the optoelectronic device that coverts terahertz signals into electric signals have received great attentions these years. Suffering from low photon energy, the development of terahertz PDs still facing significant challenges. Represented by graphene [9], black phosphorus [10], and transition metal dichalcogenides, numerous two dimensional materials have been investigated for building terahertz PDs [11–14]. However, achieving high performance PD in the terahertz range is still challenging due to the lack of the optimal combination between bandgap, dark current, and absorption capabilities. Continuous exploration of other two-dimensional materials in this field is still required.

C. Chang et al. (Eds.): YTHZ 2024, SPPHY 400, pp. 8–12, 2024.
https://doi.org/10.1007/978-981-97-3786-4_2

Adopting the characteristic of zero bandgap and high carrier density, topological semimetals (TSMs) have attracted great attentions [15]. When utilized in the fabrication of PDs, TSMs demonstrate numerous advantages, including lower dark current, ultrafast response, and low noise equivalent power. These characteristics equip them with potential applications in the far infrared and terahertz wavelength range. Among which, TSM $ZrTe_3$ have not yet been investigated.

Herein, we developed a terahertz PD adopting TSM $ZrTe_3$, utilizing the advantages of TSMs, the terahertz PD achieved high responsivity of 0.11 A/W at 0.22 THz with response time of 4.74/4.97 ms, which shows great potentials in terahertz applications. Moreover, the response range of the PD was confirmed from near infrared to terahertz, indicating the broad-band capability.

2 Results and Discussions

We designed and fabricated a $ZrTe_3$ based photodetector (PD) adopting the symmetric electrode structure. The electrode pattern was prepared through a lift-off photolithography following a thermal evaporation and deposition of 5 nm Cr and 30 nm Au on a SiO_2/Si substrate, after which the substrate was washed to remove excess metal. The $ZrTe_3$ working layer was prepared through mechanical exfoliation. The bulk crystal was exfoliated and dry transferred to the electrodes with a polydimethylsiloxane (PDMS) film. The exfoliated nanoribbon was about 100 nm thickness confirmed by atomic force microscopy (AFM) as depicted in Fig. 1a. X-ray diffraction (XRD) pattern confirms the high crystal quality of our $ZrTe_3$ as shown in Fig. 1b. Raman spectrum was also induced as shown in Fig. 1c to confirm the crystal quality, all Raman peaks corresponds well with the previous reports. In this work, the device tunnel was chosen to be 30 μm as depicted in Fig. 1d.

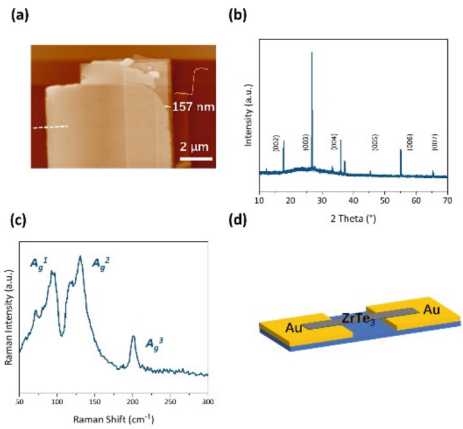

Fig. 1. Material characterization of $ZrTe_3$ (a) Atomic force microscopy (AFM) of exfoliated $ZrTe_3$ (b) X-ray diffraction (XRD) pattern (c) Raman spectrum (d) Device illustration.

We then performed basic electrical characterization on our device using a source meter (Keithly 2636B). As can be inferred from the liner *I-V* curve in Fig. 2a, our device

exhibits good ohmic contact, with the resistance of about 100 Ω. Furthermore, the noise power density spectrum were collected as Fig. 2b, at the frequency of 1 Hz, our device exhibit a relatively low noise current density of 3.73×10^{-13} A/Hz$^{1/2}$, showing great potential for building high-performance detector.

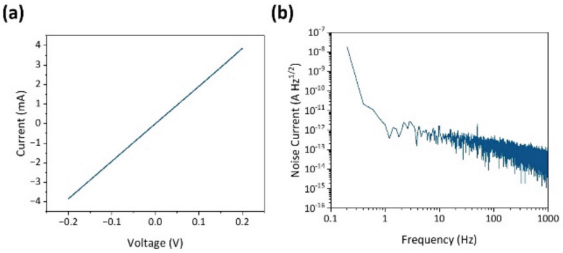

Fig. 2. Electrical characterization of ZrTe3 PD (a) I-V curve (b) noise power density spectra

Benefiting from the zero bandgap characteristics of topological semimetals, $ZrTe_3$ based PD is expected to show photon absorption capabilities across broadband even in the terahertz range with low photon energy. As demonstrated in Fig. 3a, a terahertz signal of 220 GHz (0.22 THz) with 1 Hz square wave modulation was adopted to radiate our PD directly. Under self-powered mode, our PD exhibit periodic switching of photocurrent with stability, indicating the potential of applications in terahertz range. Besides, our self-powered PD can respond to terahertz signal without antenna integration. Responsivity (R) is a figure of merit evaluating PD performance, which can be expressed as:

$$R = I_{ph}/P_{in} \tag{1}$$

where I_{ph} denotes the photocurrent generate by light signal, P_{in} denotes the efficient power of incident light, respectively. To quantitively evaluate the PD performance, we calculated the corresponding R value which is 0.11 A/W at 220 GHz. Response time is also a key figure of merit evaluating a PD performance, which defined as the time required for the photocurrent rise from 10% to 90% (t_{rise}) and decrease from 90% to 10%(t_{fall}) of peak photocurrent. As depicted in Fig. 3b, the t_{rise} and t_{fall} were 4.74 and 4.97 ms respectively, which reached a fast level in terahertz band. Noise equivalent power (NEP) is a figure of merit evaluating PD noise level, and is defined as:

$$NEP = i_n/R \tag{2}$$

where i_n is the noise current density. The lower the NEP value is, the higher the PD sensitivity is. According to the noise current spectrum recorded in Fig. 2b along with the R value, the NEP is 3.07 pW/Hz. Specific detectivity (D^*) is also a key parameter of PDs, which is defined as:

$$\mathrm{D}^* = (\mathrm{A} \times \Delta \mathrm{f})^{1/2}/\mathrm{NEP} \tag{3}$$

where A is the device effective area, Δf is the device bandwidth, respectively. Under self-powered mode at 220 GHz, our device reached a D^* of 1.49×10^9 Jones. The

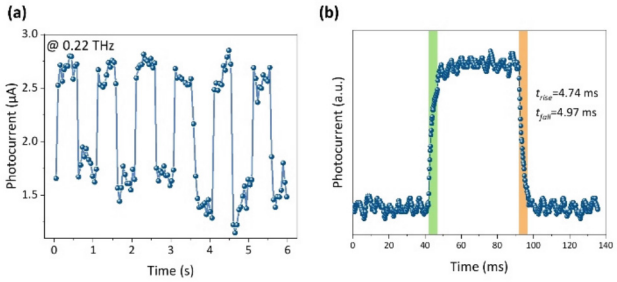

Fig. 3. Device performance of PD under 0.22 THz irradiation (a)I-t curve (b)Response time

high performance of our PD at terahertz band indicates the great potential of terahertz applications such as high-resolution terahertz imaging etc.

Adopting the zero-bandgap characteristic of ZrTe3, our PD is expected to response to broadband spectrum range. Therefore, we evaluated the photoresponse behavior of the PD from near infrared to terahertz range (0.808 μm, 1.55 μm, 4.6 μm, 10.6 μm, 12–30 μm and 1.364 μm). The corresponding *R* value are illustrated in Fig. 4, our PD exhibit peak responsivity of 0.86 A/W at 1.55 μm. Notably, we used blackbody as the light source in 12–30 μm range. The results reveal the broadband response capability of our PD, indicating the huge application potential from near infrared to terahertz.

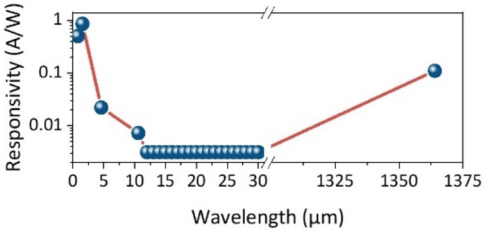

Fig. 4. Broad band detection capability: wavelength dependent responsivity of $ZrTe_3$ PD.

3 Conclusion

In summary, we designed and fabricated a topological semimetal $ZrTe_3$ based PD. The PD achieved *R* of 0.11 A/W, response time of 4.74/4.97 ms, *NEP* of 3.07 pW/Hz$^{1/2}$ and *D** of 1.49 × 10^9 Jones under self-powered mode without antenna integration at terahertz range of 220 GHz. Benefiting from the zero-bandgap characteristic, our PD exhibit broadband photoresponse capability ranging from near infrared to terahertz, reached peak responsivity of 0.86 A/W at 1.55 μm. Our finding proposed great broadband especially in terahertz range application potential of semi-metal $ZrTe_3$ based PDs.

Acknowledgement. This work was supported by the National Key Research and Development Program of China (2021YFB2800703), the National Natural Science Foundation of China (U22A2008, 62175181), the Opening Funding of National Key Laboratory of Electromagnetic Space Security, and Laoshan Laboratory Science and Technology Innovation Project (No.LSKJ202200801).

References

1. Harter, T., Füllner, C., Kemal, J.N., et al.: Generalized Kramers–Kronig receiver for coherent terahertz communications
2. Ferguson, B., Zhang, X.C.: Materials for terahertz science and technology. Nat. Mater. **1**(1), 26–32 (2012)
3. Horiuchi, N.: Terahertz technology: endless applications. Nat. Photonics **4**(3), 140 (2010)
4. Liu, G., et al.: Myelin sheath as a dielectric waveguide for signal propagation in the mid-infrared to terahertz spectral range. Adv. Funct. Mater. **29**(7), 1807862 (2019)
5. Li, Y., et al.: Terahertz wave enhances permeaility of the voltage-gated calcium channel. J. Am. Chem. Soc. **143**, 9 (2021)
6. Liu, X., et al.: Nonthermal and reversible control of neuronal signaling and behavior by midinfrared stimulation. Proc. Natl. Acad. Sci. **118**(10), e2015685118 (2021)
7. Zhang, J.X., et al.: Non-invasive, opsin-free mid-infrared modulation activates cortical neurons and accelerates associative learning. Nature Comm. **12**, 2730 (2021)
8. Xiang, Z., et al.: A primary model of THz and far-infrared signal generation and conduction in neuron systems based on the hypothesis of the ordered phase of water molecules on the neuron surface. Sci. Bull. **65**, 308 (2020)
9. Vicarelli, L., Vitiello, M.S., Coquillat, D., et al.: Graphene field-effect transistors as room-temperature terahertz detectors. Nat. Mater. **11**, 865–871 (2012)
10. Liu, C., Wang, L., Chen, X., et al.: Top-gated black phosphorus phototransistor for sensitive broadband detection. Nanoscale **10**, 5852–5858 (2018)
11. Tang, W., Liu, C., Wang, L., et al.: MoS2 nanosheet photodetectors with ultrafast response. Appl. Phys. Lett. **111**, 153502 (2017)
12. Kufer, D., Konstantatos, G.: Highly sensitive, encapsulated MoS2 photodetector with gate controllable gain and speed. Nano Lett. **15**, 7307–7213 (2015)
13. Qiu, Q., Huang, Z.: Photodetectors of 2D materials from ultraviolet to terahertz waves. Adv. Mater. **33**(15), 2008126-1-19 (2021)
14. Li, M., et al.: Ion-Bolometric Effect in Grain Boundaries Enabled High Photovoltage Response for NIR to Terahertz Photodetection. Adv. Funct. Mater. 2213970 (2023)
15. Burkov, A.A.: Topological semimetals. Nat. Mater. **15**(11), 1145–1148 (2016)

Design of an 89-183GHz Cold Optical and Quasi-Optical System

Jia-Hui Li[1,2(✉)], Hao-Tian Zhu[1,2], and Guang Liu[1]

[1] National Space Science Center, Chinese Academy of Sciences, Beijing 100190, China
lijiahui221@mails.ucas.ac.cn
[2] University of Chinese Academy of Sciences, Beijing 100049, China

Abstract. According to the basic principles of quasi-optical and gaussian beam, the quasi-optical mirror and lens are studied, and a set of millimeter-wave antenna quasi-optical feed system is designed, which can realize two channels of 89–183 GHz to receive electromagnetic radiation signals at the same time. The quasi-optical calculation and preliminary results are completed. The system works in low-temperature Dewar, in view of the actual needs, the locations and beam radius of the quasi-optical device are constrained and continuously optimized.

Keywords: Ellipsoidal reflector · Parabolic reflector · Quasi-optical · Terahertz

1 Introduction

Quasi-optical technology has become an important branch of millimeter-wave and terahertz science and technology, this technology has the characteristics of low-loss, high power, multi-polarization and wide frequency band [1]. The back-end of this design is the receiver of terahertz radiometer. The LNA of the back-end circuit works at a temperature of 20K, and a SIS mixer is used, which works at a temperature of 4K. The whole system works in a low temperature Dewar, and the whole quasi-optical system transits from 300 K to 4 K. According to the constraints of cold optical, it is necessary to reasonably arrange the different locations of the quasi-optical components in the Dewar and reduce the window size to reduce the heat leakage.

2 Quasi-Optical Design Principle

2.1 Gaussian Beam

Gaussian beam theory is the basis of quasi-optical system design. It is a transmission equation obtained by Helmholtz wave equation under the condition of paraxial approximation, which can be expressed as

$$E(r,z) = \sqrt{\frac{2}{\pi\omega_0}}\exp\left(-\frac{r^2}{\omega^2} - jkz - j\frac{\pi r^2}{\lambda R} + j\varphi_0\right) \quad (1)$$

C. Chang et al. (Eds.): YTHZ 2024, SPPHY 400, pp. 13–18, 2024.
https://doi.org/10.1007/978-981-97-3786-4_3

where r is the vertical distance from the propagation axis, ω is the beam radius of the Gaussian beam, R is the wavefront curvature radius of the Gaussian beam, φ_0 is the phase shift, and ω_0 is the beam waist of the Gaussian beam, that is, the beam radius at z = 0. Figure 1 shows the Gaussian beam propagating along the z-axis [2].

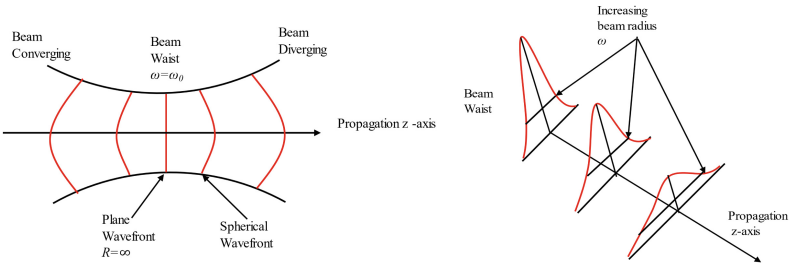

Fig. 1. Schematic of gaussian beam propagating.

2.2 Reflectors and Lenses

ABCD matrix is an important method to solve the beam transformation problem of quasi-optical system [3]. For a thin lens with refractive index n, its ABCD matrix is

$$M = \begin{bmatrix} A & B \\ C & D \end{bmatrix} = \begin{bmatrix} 1 & 0 \\ -\frac{1}{f} & 1 \end{bmatrix} = \begin{bmatrix} 1 & 0 \\ -(n-1)\left(\frac{1}{R_1}+\frac{1}{R_2}\right) & 1 \end{bmatrix} \tag{2}$$

where R_1 and R_2 are the radius of curvature of the left and right surfaces respectively. For ellipsoidal reflector and parabolic reflector, they can be equivalent to a lens system. The key to design is to find their equivalent focal length f. For ellipsoidal reflector, equivalent focal length is

$$f_e = \frac{R_1 R_2}{R_1 + R_2} \tag{3}$$

A common scheme is: when R_1 is equal to the distance from the ellipsoidal focus F_1 of the ellipsoidal reflector to the incident point and R_2 is equal to the distance from F_2 to the outgoing point, the incident beam and the outgoing beam match[4]–[6].

For parabolic reflector with an incident angle of 45°, equivalent focal length is

$$f_p = \frac{R}{2} \tag{4}$$

Figure 2 shows the corresponding figures of the parameters of the ellipsoidal mirror and the parabolic mirror. Note that d_1 and d_2 are the distance from the waist of the incident beam to the mirror and the distance from the waist of the outgoing beam to the mirror, respectively.

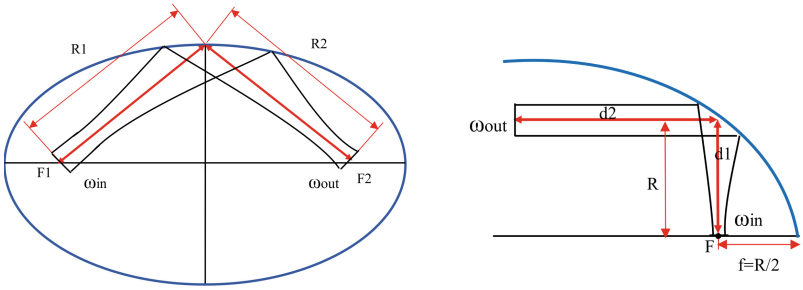

Fig. 2. Schematic of gaussian beam transformation (a) ellipsoidal mirror (b) parabolic mirror

3 Quasi-Optical Design

Firstly, considering the compactness of the optical path layout, two channels with relatively close frequencies can be multiplexed. The 89/110–115 GHz channel is received by a corrugated horn, and the 183 GHz channel is received by another corrugated horn. The system works in a low-temperature Dewar, and it is necessary to comprehensively consider the Dewar window size constraint and the mirror size constraint, and adjust the optical path space layout and the Gaussian beam radius to make the optical path structure reasonable and satisfy the constraints. In the far field, the relative field distribution of the Gaussian beam can be expressed as.

$$\frac{E(r)}{E(0)} = \exp[-(\frac{r}{\omega})^2] \tag{5}$$

where E(r) represents the electric field intensity at r from the Gaussian beam axis, E(0) represents the electric field intensity on the Gaussian beam axis at the same section, r is the intercept radius, and ω is the beam radius of the Gaussian beam. It should be noted that the beam radius corresponds to only 86.5% of the energy. We select 1.8 times the beam radius for design, about 99.85% [7].

The diagram of the Dewar structure is shown in Fig. 3(b). Layout is shown in Fig. 3(a). The 89/110–115 GHz frequency component is completely transmitted, and the 183 GHz frequency component is completely reflected. Finally, each frequency signal is received by the corresponding channel horn feed.

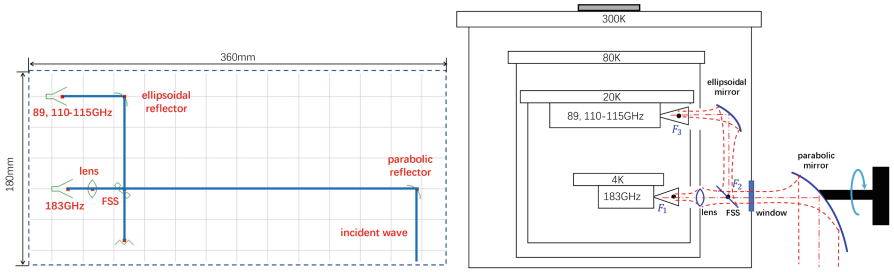

Fig. 3. (a) Quasi-optical network layout (b) Schematic of dewar structure

4 Quasi-Optical System Simulation

The design parameters of ellipsoidal mirror and parabolic mirror are shown in Table 1. The calculated results of the normalized pattern are shown in Fig. 4. Results of quasi-optical system are shown in Table 2.

Table 1. Parameters of the reflector

Reflector	Focal length	Distance of R_1	Distance of R_2
ellipsoidal	49.9 mm	65.9 mm	205.4 mm
parabolic	299.8 mm	299.8 mm	inf

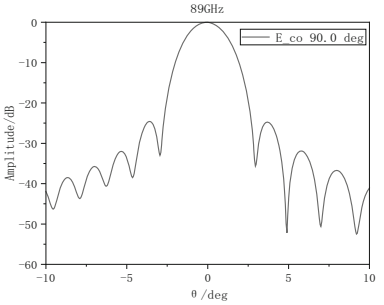

(a) 89 GHz beam radiation pattern(E-plane)

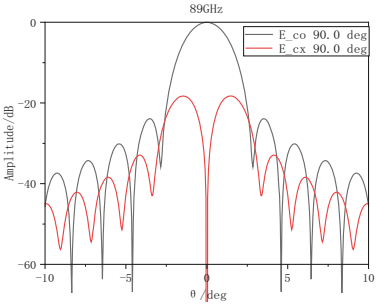

(b) 89 GHz beam radiation pattern(H-plane)

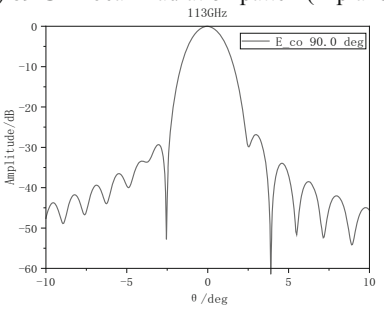

(c) 113 GHz beam radiation pattern(E-plane)

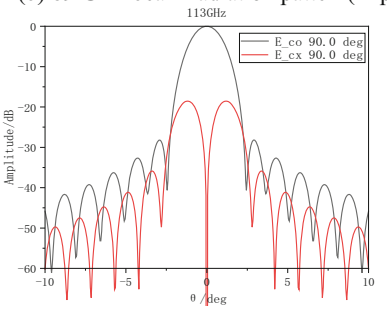

(d) 113 GHz beam radiation pattern(H-plane)

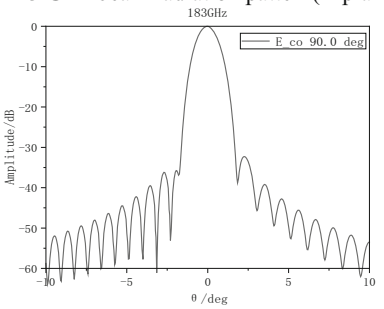

(e) 183 GHz beam radiation pattern(E-plane)

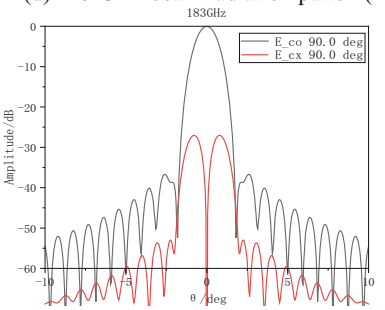

(f) 183 GHz beam radiation pattern(H-plane)

Fig. 4. Far-field normalized radiation pattern of each frequency channel

Table 2. Results of quasi-optical system

Frequency (GHz)	Directivity	Beam width(-3dB)	Main beam efficiency	Side lobe levels	Polarization purity
89	39.3dB	2.2°	99%	−24.6dB	18.3dB
113	41.1dB	1.8°	98.9%	−26.9dB	18.6dB
183	44.6dB	1.2°	99.1%	−32.3dB	27dB

5 Conclusion

According to the actual requirements and constraints, after many modifications and improvements, the quasi-optical path of 89–183 GHz system is designed theoretically and simulated. Follow-up work will continue to optimize and improve according to the requirements of the engineering.

Acknowledgments. The authors would like to thank Dr. Dong Liu, an Associate Researcher with Purple Mountain Observatory, Chinese Academy of Sciences, China, for providing useful suggestions of the quasi-optical design. This work was fully supported by the National Key R&D Program of China under Grant 2023YFB3905603.

References

1. Liu, X., et al.: Quasi-optical technology in the millimeter and terahertz wave ranges: theory, applications and development. J. Terahertz Sci. Elect. Inform. Tech. **22** 631–652 (2022)
2. Whale, M.: Optical Characterisation of Astronomical Submillimetre Receivers Including ALMA Bands 5 and 9. National University of Ireland Maynooth, Diss (2010)
3. Goldsmith, P.F.: Quasi-optical techniques. Proc. IEEE **80**(11), 1729–1747 (1992)
4. Liu, G., et al.: Myelin sheath as a dielectric waveguide for signal propagation in the mid-infrared to terahertz spectral range. Adv. Funct. Mater. **29**(7), 1807862 (2019)
5. Li, Y., et al.: Terahertz wave enhances permeability of the voltage-gated calcium channel. J. Am. Chem. Soc. **143**(11), 4311–4318 (2021)
6. Yao, C., et al.: A ten frequency bands quasi optical feed network. J. Terahertz Sci. Electron. Inf. Technol. **21**(2), 139–142 (2023)
7. Li, B., et al.: Research progress in terahertz quasi-optical feed network. J. Terahertz Sci. Electron. Inf. Technol. **17**(6), 939–943 (2020)
8. Liu, J., et al.: Design and analysis of the quasi-optical feed system. J. Terahertz Sci. Electron. Inf. Technol. **18**(2), 4 (2020)
9. Li, B., et al.: Terahertz quasi-optical feed network system optimization method. J. Detect. Control **44**(5), 112–115 (2022)

A Compact Graphene-Based Hot Electron Bolometer System for Terahertz Radiation Detection

Feiming Li[1,2], Wei Miao[1(✉)], Qingcheng Wang[1,2], Cui Yu[3], Zezhao He[3], Jiaqiang Zhong[1], Feng Wu[1], Zheng Wang[1], Kangmin Zhou[1], Yuan Ren[1], Wen Zhang[1], Jing Li[1], Shengcai Shi[1], Qingbin Liu[3], and Zhihong Feng[3]

[1] Purple Mountain Observatory, Chinese Academy of Sciences, Nanjing 210033, China
weimiao@pmo.ac.cn
[2] University of Science and Technology of China, Hefei 230026, China
[3] National Key Laboratory of Soild-State Microwave Devices and Circuits, Shijiazhuang 050051, China

Abstract. In this paper, we present the development of a compact hot electron bolometer (HEB) system for terahertz radiation detection. The bolometer system integrates a graphene-based HEB as its core detection unit and employs a compact infrared Dewar for efficient cooling of the graphene-based HEB. Utilizing 300 K/77 K loads as calibration sources, we quantified the sensitivity of the bolometer system at 4.2K. The measured results demonstrate a moderate sensitivity, with a noise equivalent power (NEP) of approximately 3.3×10^{-12} W/Hz$^{0.5}$. Furthermore, we evaluated the bolometer system's response time by applying a modulated terahertz signal, and the measured response time is found to be approximately 1 μs. These results underscore the promising potential of our graphene-based HEB bolometer system, especially in applications that require sensitive and high-speed detection capabilities.

Keywords: Terahertz · Compact · Graphene-based HEB · Noise equivalent power · Response time

1 Introduction

In recent years, there has been rapid development in the field of graphene, emerging as a prominent two-dimensional material. Due to its unique electronic structure, graphene exhibits distinct characteristics such as low electron heat capacity [1], weak electron-phonon interactions [2], and high electron mobility [3]. Moreover, its consistent absorption intensity across mid-infrared to ultraviolet wavelengths makes graphene well-suited for detector applications [4]. However, the relatively weak dependence of graphene resistance on temperature necessitates researchers to enhance this dependency through various methods for effective detection [5, 6]. An encouraging alternative, Johnson noise readout [7], stands out as it doesn't demand a strong resistance-temperature relationship

C. Chang et al. (Eds.): YTHZ 2024, SPPHY 400, pp. 19–23, 2024.
https://doi.org/10.1007/978-981-97-3786-4_4

or additional bias sources, allowing the detector to operate at the required temperature. This method facilitates the investigation of detector thermal transport properties, elucidation of their physical mechanisms, and provides guidance for detector development [8]. Although detectors employing Johnson noise readout have been demonstrated, the compactness of the detector systems is crucial for practical applications, especially for bio-information detection [9, 10]. To achieve system compactness, we integrated a graphene-based hot electron bolometer (HEB) and a low-temperature low-noise amplifier into a 4.2 K infrared Dewar. We determined the noise equivalent power of bolometer system by using 300 K/77 K loads as calibration sources, and characterized the response time by applying a modulated THz signal to the graphene-based HEB. Additionally, we compared our results with a commercial silicon-based bolometer.

2 Bolometer System

The bolometer system mainly consists of an HEB, a low-temperature low-noise amplifier, a thermometer, a room-temperature amplifier, a square-law detector, and a compact infrared Dewar. Figure 1a shows a SEM image of the graphene-based HEB, consisting primarily of a spiral antenna and a graphene microbridge. The frequency range of the spiral antenna is 0.3–1.6 THz, which is used to absorb radiation signals. The graphene microbridge has dimensions of 0.4 μm in length and 3 μm in width, and it is fabricated using epitaxial growth of bilayer graphene, as described in Refs. 11 and 12. Superconducting material Nb was used as electrodes connected to graphene to enhance detector performance by suppressing electron diffusion due to Andreev reflection. Subsequently, the graphene-based HEB was mounted on an elliptical high-resistance silicon lens used to collect THz radiation and placed in an oxygen-free copper block connected to the cold plate of the infrared Dewar. A low-temperature low-noise amplifier (1–12 GHz) and a thermometer were also placed in the infrared Dewar, as shown in Fig. 1d. Here, the low-temperature low-noise amplifiers are used to amplify detection signals, and the thermometer was used to monitor the temperature of the cold plate to ensure that the bolometer system operates at the correct temperature. The transmission between the HEB and low-temperature low-noise amplifier is achieved through CPWG structured transmission line, as shown in Fig. 1b. In order to ensure effective signal transmission, the design was carried out using the commercial software package HFSS based on finite element method to simulate the transmission line. The specific parameters are shown in Table 1. The simulation results are shown in Fig. 1c, and it can be seen that there is still good transmission characteristics at 12 GHz, which meets the requirements of the experiment. Figure 1e depicts the graphene-based HEB system with Johnson noise readout. After assembling the internal system of the Dewar, we further amplified the signal using room-temperature amplifiers (1–8 GHz) and detected the signal using a square-law detector. Additionally, impedance matching is a crucial issue to ensure the efficient operation of the system. According to the formula $\eta = (4R_0R_L)/(R_0 + R_L)^2$, we evaluated the efficiency between the detector and the low-temperature low-noise amplifier to be 97%, here the resistance measured experimentally at 4.2 K was approximately 36 Ω, thus allowing us to ignore the effects of reflection.